Check for updates

# Spatiotemporal variability of soil-water characteristic curve model parameters of Lanzhou collapsible loess

Wenju Zhao [a,*], Yuhang Liu[a], Jiazhen Hu[a] and Zongli Li[b]

[a] College of Energy and Power Engineering, Lanzhou University of Technology, Lanzhou 730050, China
[b] General Institute for Water Resources and Hydropower Planning and Design, Ministry of Water Resources, Beijing 100120, China
*Corresponding author. E-mail: wenjuzhao@126.com

WZ, 0000-0001-6204-1842

## ABSTRACT

The spatiotemporal variation of the model parameters of the soil-water characteristic curve (SWCC) reflect the soil water holding capacity and soil pore distribution state. It is an integral part of interdisciplinary disciplines such as soil hydrodynamics and ecohydrology. The authors selected the optimal SWCC model for the Lanzhou collapsible loess, used classical statistics and geostatistics methods to study the spatio-temporal variability of the SWCC model parameters, and using the comprehensive comparison of the mean relative differences (MRD), standard deviations (SDRD) and an index of temporal stability (ITS) determined the representativeness measuring point. The results showed that the SWCC parameter $\alpha$ was medium variability in the 0–30 cm soil layer, $n$ and $\theta_s$ were of low variability, and the spatial distribution of the parameters of different soil layers was consistent. Migration direction prediction of $\theta_s$ was very similar in each layer, $\alpha$, $n$ and $\theta_s$ were all strongly significantly correlated positively. Moreover, the determination coefficient of representative measuring point 16 had the highest prediction accuracy for the measured values of SWCC. The results of this paper can be used as a simple method to predict SWCC and provide theoretical guidance for soil water management and soil collapse erosion monitoring in the collapsible loess area.

Key words: collapsible loess, prediction, soil-water characteristic curve, spatial variability, temporal stability

## HIGHLIGHTS

- A study is presented of the temporal stability and variability of SWCC in the Lanzhou collapsible loess, using the comprehensive comparison of the mean relative differences (MRD), standard deviations (SDRD) and an index of temporal stability (ITS), and the representativeness measuring point was determined.
- The SWCC parameter $\alpha$ is medium variability in the 0–30 cm soil layer, n and $\theta_s$ are of low variability. The spatial distribution of the SWCC parameters was consistent. Migration direction prediction of $\theta_s$ was very similar in each layer. $\alpha$, n and $\theta_s$ were all strongly significantly correlated positively.
- A small amount of observations was used to monitor SWCC on a large scale, providing a fast and effective monitoring method for soil erosion in the Loess Plateau.

## INTRODUCTION

Collapsible loess is widely distributed worldwide, accounting for about one-tenth of the global land area (Li *et al.* 2019; Ostad-Ali-Askari *et al.* 2018b). The sensitivity of the hydro-mechanical properties of loess deposits contributes to various problems including the differential settlement (Ostad-Ali-Askari *et al.* 2018a, 2018b; Derakhshannia *et al.* 2020), landslides (Yan & Wen 2013), which can in turn damage infrastructure and even cause casualties of the loess region areas of China (Zhang & Peng 2015; Haeri *et al.* 2019). Numerous studies were conducted to better understand the influence of collapsibility and the stability of slopes in loess deposits from the mechanism. Ng *et al.* (2017) studied the mechanism from the aspects of micro-structure, mechanics and temperature. Xing *et al.* (2007) believed that the collapsibility of loess was mainly due to the reduction of soil strength and to structural damage from water absorption. Loess is mainly distributed among China in the northwest, where the climate is dry, rainfall is low and the loess is generally unsaturated. The study of the mechanism of collapse of loess based on the theory of unsaturated soil mechanics therefore has high theoretical and application value.

The soil-water characteristic curve (SWCC) defines the relationship between water content and matrix suction in unsaturated soil (saturation, Sr, mass water content, $\omega$, or volumetric water content, $\theta$) (Wang *et al.* 2017; Zhao *et al.* 2020), which is widely used in geotechnical, geo environmental, and agricultural engineering (Wang *et al.* 2017). SWCC is a fundamental element for characterizing the essential aspects of unsaturated soil behavior and it plays an important role in unsaturated soil mechanics. The estimation of the soil-water characteristic curve (SWCC) is currently the main method. Experts and scholars have developed several empirical formulas to represent SWCC, such as the Van Genuchten (VG) model (Lin & Xu 2018) and the Gardner model (Zhang *et al.* 2019). Among these, the VG model has been widely used because of its good fit with measured data (Liu *et al.* 2007). Therefore, this paper selects the VG model with good applicability, high precision, and clear physical meaning. Olyphant (2003) found that the VG model parameters of sand basically showed a steady-state change trend over time, but abnormal values appeared before the end of the monitoring period. Chen (2004) obtained an SWCC for slopes in a small watershed in the gully region of the Loess Plateau, which had some amount of spatial variability. Idrysy & Smedt (2007) better predicted the spatial variation of hydraulic conductivity by using hydraulic gradients and Kriging spatial interpolation.

Using SWCC to indirectly derive the permeability coefficient of unsaturated loess has great randomness (Wen *et al.* 2015). The concept of temporal stability; that is, the preservation of spatial patterns of SWC over time, was introduced by Vachaud *et al.* (1985). Zucco *et al.* (2014); Zhao *et al.* (2017) successfully identified representative sample points that remained stable over time and estimated the average SWC in the field. Coppola *et al.* (2011) found that the average water saturation affects the temporal stability of the spatial distribution of soil moisture in farmland. The spatiotemporal variability of SWCC has been well studied, but these studies have mainly focused on weak expansive soil, calcareous soil, weathered granite residual soil, gravel-mulched fields (Yun-Xue *et al.* 2019; Lv *et al.* 2021; Shen *et al.* 2021). Little is known about the validity of the concept for Collapsible Loess in northwestern China. The objective of the study is to analyze the temporal stability, spatial variation and determine the representative measurement points of SWCC parameters in collapsible loess using the mean relative differences (MRD), standard deviation (SDRD), index of temporal stability (ITS). A more descriptive understanding of the spatiotemporal patterns of SWCC can further be provided. The findings can be used as a simple method to predict SWCC and provide theoretical guidance for soil water management and soil collapse erosion monitoring in collapsible loess area…

## MATERIALS AND METHODS

### Description of the study area

The experimental soil samples were collected from the Peng jia ping campus of Lanzhou University of Technology in Lanzhou City, Gansu Province, China (35°50′–36°06′N and 103°36′–103°54′E) (Figure 1), located in the transitional area from the Qinghai-Tibet Plateau to the Loess Plateau, belonging to the Yellow River Basin. This area is a typical loess landform in China. The climate is temperate continental climate, with an average annual sunshine duration of 2,446 h and an average
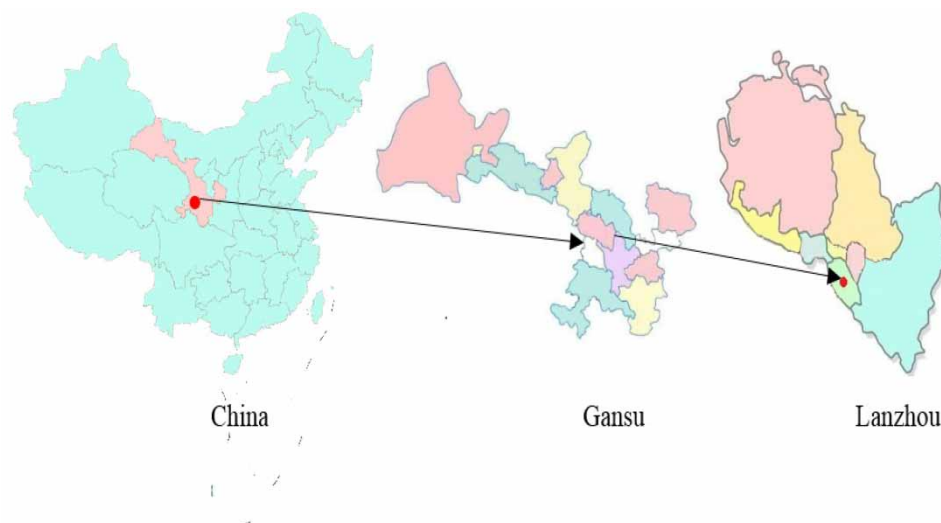


**Figure 1** | Study area and the soil sampling locations in the study area situated in Gansu, China.

frost-free period of $>180$ days. The annual average temperature is between 6.4 and 11.2 °C, the annual precipitation is between 276.4 and 494.2 mm, and the rainfall is mainly concentrated in June to September. Grey cinnamon soil, lime calcite soil, and chestnut soil are the predominant soils in this area.

## RESEARCH METHODS

### Field sampling

The soil texture of the study site is silty clay loam, with an area of $80 \times 80$ m. The sampling time was from July 2019 to November 2019, and from July 2020 to November 2020. The mechanical spot sampling scheme was adopted for all samples, and all samples were then collected using stainless-steel cutting rings (5 cm in height by 5 cm in diameter) from the 0–10, 10–20, 20–30 cm layers. The samples were collected from the 0 to 30 cm layers in 16 evenly distributed $4 \times 4$ m quadrants 20 m apart, center to center (Figure 2). The ring bulk method was used to measure the bulk density at each point due to the widespread distribution of the samples and the convenience of centralized management. The excavations were then manually filled based on the actual bulk densities. All collected soil samples were air-dried, sieved through a 2 mm sieve and then loaded into 100 cm³ cutting rings in layers based on the measured bulk density. The dry bulk density was 1.58 g/cm³. A Nissan CR21GII high-speed constant-temperature refrigerated centrifuge was used to determine the SWCC at a constant temperature of 4 °C. Before the start of the experiment, the soil samples collected with the special cutting ring of the centrifuge were placed in water for saturation treatment, balanced with a balance and placed symmetrically in the centrifuge rotor, the suction range was set from 0 to 7,000 cm. After the centrifugation was completed and cooled, use weighing method to measure volumetric soil water content (SWC), each treatment was repeated 3 times, and the average value was taken as the result.

$$\theta_w = \frac{w}{\gamma_d} \tag{1}$$

where $\theta_w$ is the volumetric water content (cm³/cm³); $\gamma_d$ is dry bulk density; $w$ is the mass water content.

### Data analysis

The temporal stability, spatial variation and the representative measurement points of SWCC parameters were analyzed using the Mean relative differences (MRD), standard deviation (SDRD), index of temporal stability (ITS) with Origin11.0, Surfer and other software.

The Van Genuchten (VG) model is:

$$\theta(h) = \begin{cases} \theta_r + \dfrac{\theta_s - \theta_r}{(1 + |\alpha h|^n)^m} & h < 0 \\ \theta_s & h \geq 0 \end{cases}. \tag{2}$$

where $\theta$ is the volumetric water content (cm³/cm³), $\theta_s$ is the saturated volumetric water content (cm³/cm³), $\theta_r$ is the residual volumetric water content (cm³/cm³), $h$ is the pressure head (m), $\alpha$ is a scaling parameter that is inversely proportional to mean pore diameter, $m$ and $n$ are shape coefficients, where $m = 1 - 1/n$ or $m = 1 - 2/n$, the authors use $m = 1 - 1/n$ (Genuchten V 1980; Lin & Xu 2018). The value of $n$ determines the slope of the SWCC. When $n$ is large, the slope is
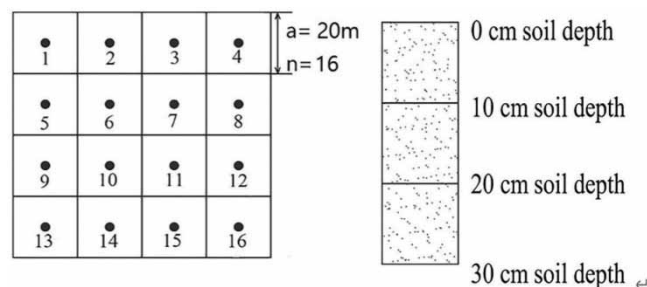


**Figure 2** | Distribution map of sampling points (note: a is mesh size and n is total sampling points).

large, and when $n$ is small, the slope is small.

$$CV_j = \frac{s_j}{\bar{x}_j} = \frac{\sqrt{\frac{1}{n-1}\sum_{i=1}^{n}(x_{ij} - \bar{x}_j)^2}}{\bar{x}_j} \tag{3}$$

where $s_j$ is the standard deviation of the site on day $j$. Then $x_i$ is the parameter of SWCC of the $i$ measuring points at $j$. $\bar{x}_j$ is the average value of the SWCC parameter of all the $j$ measuring points. $CV_j$ is the coefficient of variation ($CV$) of each sampling day. A $CV_j < 10\%$ indicates low variation, $10\% < CV_j \leq 100\%$ indicate moderate variation and a $CV_j > 100\%$ indicates high variation (Wraith 2004).

Geostatistical methods

Based on the regionalized variables theory and intrinsic hypothesis, the semivariogram, $\gamma$(h), was estimated by Pham (2016):

$$\gamma h = \frac{1}{2N(h)}\sum_{i=1}^{N(h)}[Z(x_i + h) - Z(x_i)]^2 \tag{4}$$

where $h$ is the spatial sampling interval, $\gamma h$ is the semivariance for interval $h$, $N(h)$ is the total number of sample pairs for the separation interval $h$, and $Z(x_i + h)$ and $Z(x_i)$ are measured samples at points $x_i + h$ and $x_i$, respectively.

Relative deviation is used to analyze the time stability characteristics of a single observation point. It describes the relationship between a single observation point and the average of all observation points. It was first proposed by Vachaud *et al.* (1985):

$$\delta_{ij} = (x_{ij} - \overline{x_j})/\overline{x_j} \tag{5}$$

where $\delta_{ij}$ is the value of relative deviation at time $j$ ($j = 1,2,\ldots\ldots,n$) at point $i$ ($i = 1,2,\ldots\ldots,n$), and $\bar{x}_j$ is the average value of SWCC parameter of all the $j$ measuring points.

Mean relative difference (MRD):

$$\overline{\delta_i} = \frac{1}{m}\sum_{j=1}^{m}\delta_{ij} \tag{6}$$

where $m$ is the number of samples, $\overline{\delta_i}$ is the average value of $\delta_{ij}$.

The standard deviation of MRD (SDRD):

$$\delta(\delta_i) = \sum_{j=1}^{m}(\frac{\delta_i - \overline{\delta_i}}{m-1})^{1/2} \tag{7}$$

where $\delta(\delta_i)$ is the standard deviation of $\overline{\delta_i}$.

Regional average $x$ is estimated by measuring points with MRD close to 0 and lowest standard deviation. The index of time stability (ITS) is considered to identify the representative measuring points of the average soil moisture in the field. ITS is a combination of the average relative deviation and its standard deviation. It is proposed by Jacobs *et al.* (2010):

$$ITS_i = (\overline{\delta_i}^2 + \delta(\delta_i)^2)^{1/2} \tag{8}$$

where $ITS_i$ is the index of time stability.

## RESULTS AND DISCUSSION

### Statistical analysis of soil-water characteristic function

The SWCC model parameters of the soil in the 0–30 cm soil layers at each sampling point were counted. The statistical results showed that the coefficient of variation (*CV*) of parameter $\alpha$ (the scaling parameter that is inversely proportional to mean pore diameter) is greater than that of parameter $\theta_s$ (the saturated volumetric water content) and $n$ (shape coefficients, the value of $n$ determines the slope of the SWCC, when $n$ is large, the slope is large, and when $n$ is small, the slope is small), *CV* of $\alpha$ is between 10.19% and 22.36% which indicates moderate variation. The next most influential was $n$, which indicates low variation. The $\theta_s$ had the smallest influence and indicates low variation (Table 1). *CV* tended to decrease as mean $\theta_s$ increased for all layers, in accordance with most previous studies of $\theta_s$ spatial variability (Brocca *et al.* 2012). This is because higher surface $\theta_s$ may be the result of soil surface evaporation and plant root water absorption. At the same time, environmental factors such as rainfall and infiltration will make surface *CV* stronger than its lower layer. However, *CV* tended to increase as mean $\theta_s$ increased for all layers (Penna *et al.* 2013; Vanani *et al.* 2017). This is different from our results, which may have been due to study area, the topography or sand content.

The parameter $\alpha$ did not differ significantly between the layers, but the average fitting tended to decrease with depth. The size distribution of the soil particles was 12.88% gravel, 66.58% silt and 20.54% clay for the 0–10 cm layer, 11.03% gravel, 67.32% silt and 21.65% clay for the 10–20 cm layer and 9.59% gravel, 67.14% silt and 23.27% clay for the 20–30 cm layer. Clay content increased, the intake value of the characteristic curve increased and the fitting parameter $\alpha$ accordingly decreased with depth. $\theta_s$ was correlated strongly with the change of season. $\theta_s$ was low in November, but significantly higher in July, because the region receives more rainfall in July.

### Spatial variability of the SWCC parameters

#### SWCC parameters distribution in different soil layers

The authors used geostatistical Kriging interpolation (Oliver & Webster 2014) in Surfer to draw the spatial distribution maps of SWCC parameters to a depth of 30 cm (Figure 3) and to more intuitively explore the characteristics of the spatial distribution of the parameters at different depths. The soil-water suction measured using a centrifuge was processed by the flow-direction analysis tool in Surfer. The soil-water suction was used as the driving force of the SWCC parameters. The direction of flow obtained from the soil-water suction can approximately represent the prediction of the direction of migration of parameters; the longer the arrow, the stronger the driving force.

The distribution of the SWCC parameters was consistent in different space and time (Figure 3). This result indicated that the SWCC for a specific layer could be estimated using data from adjacent soils, thereby reducing the waste of human and financial

**Table 1** | VG characteristic curve parameter statistics

| Time | Soil layer (cm) | Parameter | MAX | MIN | AVE | SD | CV |
|------|-----------------|-----------|-----|-----|-----|-----|-----|
| **2019/7** | 0–10 | $\alpha$ | 0.0116 | 0.0059 | 0.0079 | 0.0016 | 19.77% |
| | | $n$ | 2.2326 | 1.2164 | 1.6116 | 0.2141 | 13.29% |
| | | $\theta_s(\mathrm{cm^3/cm^3})$ | 0.5616 | 0.4925 | 0.5121 | 0.0178 | 3.48% |
| | 10–20 | $\alpha$ | 0.0093 | 0.0044 | 0.0062 | 0.0014 | 22.36% |
| | | $n$ | 2.4101 | 1.6074 | 2.0564 | 0.2839 | 13.81% |
| | | $\theta_s(\mathrm{cm^3/cm^3})$ | 0.5580 | 0.4959 | 0.5145 | 0.0170 | 3.30% |
| | 20–30 | $\alpha$ | 0.0078 | 0.0044 | 0.0062 | 0.0009 | 15.20% |
| | | $n$ | 2.4862 | 1.6549 | 1.8319 | 0.1938 | 10.58% |
| | | $\theta_s(\mathrm{cm^3/cm^3})$ | 0.5520 | 0.4962 | 0.5149 | 0.0133 | 2.59% |
| **2019/11** | 0–10 | $\alpha$ | 0.0035 | 0.0024 | 0.0028 | 0.0003 | 11.74% |
| | | $n$ | 3.3907 | 2.3914 | 2.9263 | 0.2597 | 8.87% |
| | | $\theta_s(\mathrm{cm^3/cm^3})$ | 0.4510 | 0.4171 | 0.4312 | 0.0081 | 1.88% |
| | 10–20 | $\alpha$ | 0.0034 | 0.0024 | 0.0027 | 0.0003 | 10.34% |
| | | $n$ | 3.5870 | 2.5475 | 2.9498 | 0.2662 | 9.03% |
| | | $\theta_s(\mathrm{cm^3/cm^3})$ | 0.4512 | 0.4205 | 0.4319 | 0.0081 | 1.87% |
| | 20–30 | $\alpha$ | 0.0033 | 0.0023 | 0.0026 | 0.0003 | 10.19% |
| | | $n$ | 3.3469 | 2.3125 | 2.8929 | 0.2722 | 9.41% |
| | | $\theta_s(\mathrm{cm^3/cm^3})$ | 0.4521 | 0.4208 | 0.4322 | 0.0078 | 1.81% |
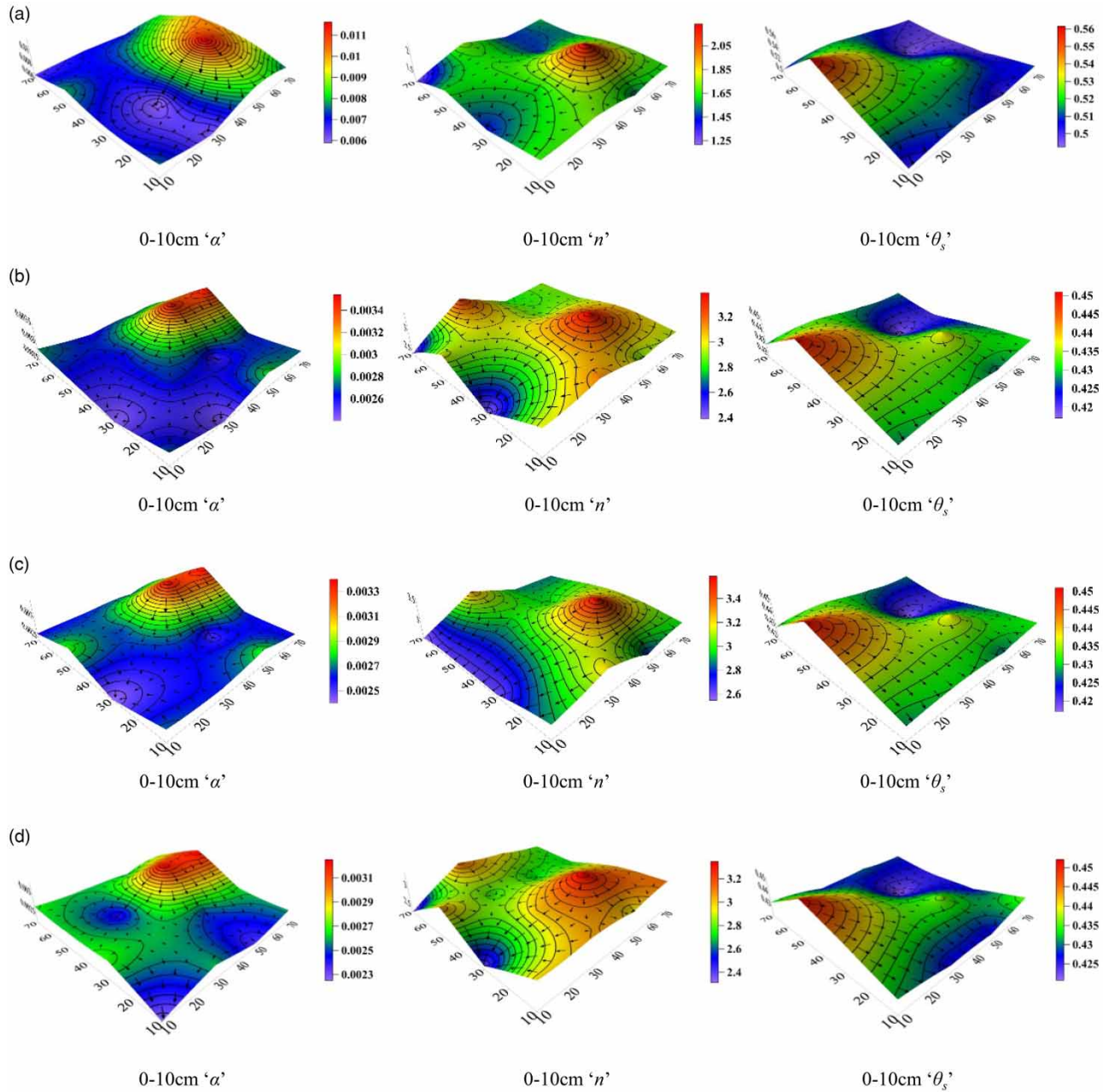
**Figure 3** | Spatial distribution map of SWCC parameters (Note: a represents the sample of July 2019; b, c, d represents the sample of November 2019; the arrows indicate the migration direction).

**Table 2** | Correlation between SWCC parameters and different soil depth

| Parameter | $\alpha$ | | | $n$ | | | $\theta_s$/(cm³/cm³) | | |
|---|---|---|---|---|---|---|---|---|---|
| Soil layer (cm) | 0–10 | 10–20 | 20–30 | 0–10 | 10–20 | 20–30 | 0–10 | 10–20 | 20–30 |
| **0–10** | 1 | 0.842** | 0.749** | 1 | 0.905** | 0.823** | 1 | 0.977* | 0.967* |
| **10–20** | | 1 | 0.937** | | 1 | 0.920** | | 1 | 0.979* |
| **20–30** | | | 1 | | | 1 | | | 1 |

*Note*: **indicates a significant correlation at the 0.01 level, *indicates a significant correlation at the 0.05 level.

resources. The $\theta_s$ increases with the increase of soil depth at 0–30 cm, with ranges of 0.4171–0.4510, 0.4205–0.4512 and 0.4208–0.4521 for the 0–10, 10–20, 20–30 cm layers, respectively. The predicted direction of migration of parameters was the same in each layer, indicating that the area was less affected by humans. Parameters migrated from high to low under the effect of the matrix potential gradient. Comparing the statistical results of July and November 2019, the range of the parameter $\theta_s$ on the 0–10 cm soil layer further proves that the sampling time is different and the model parameters are quite different.
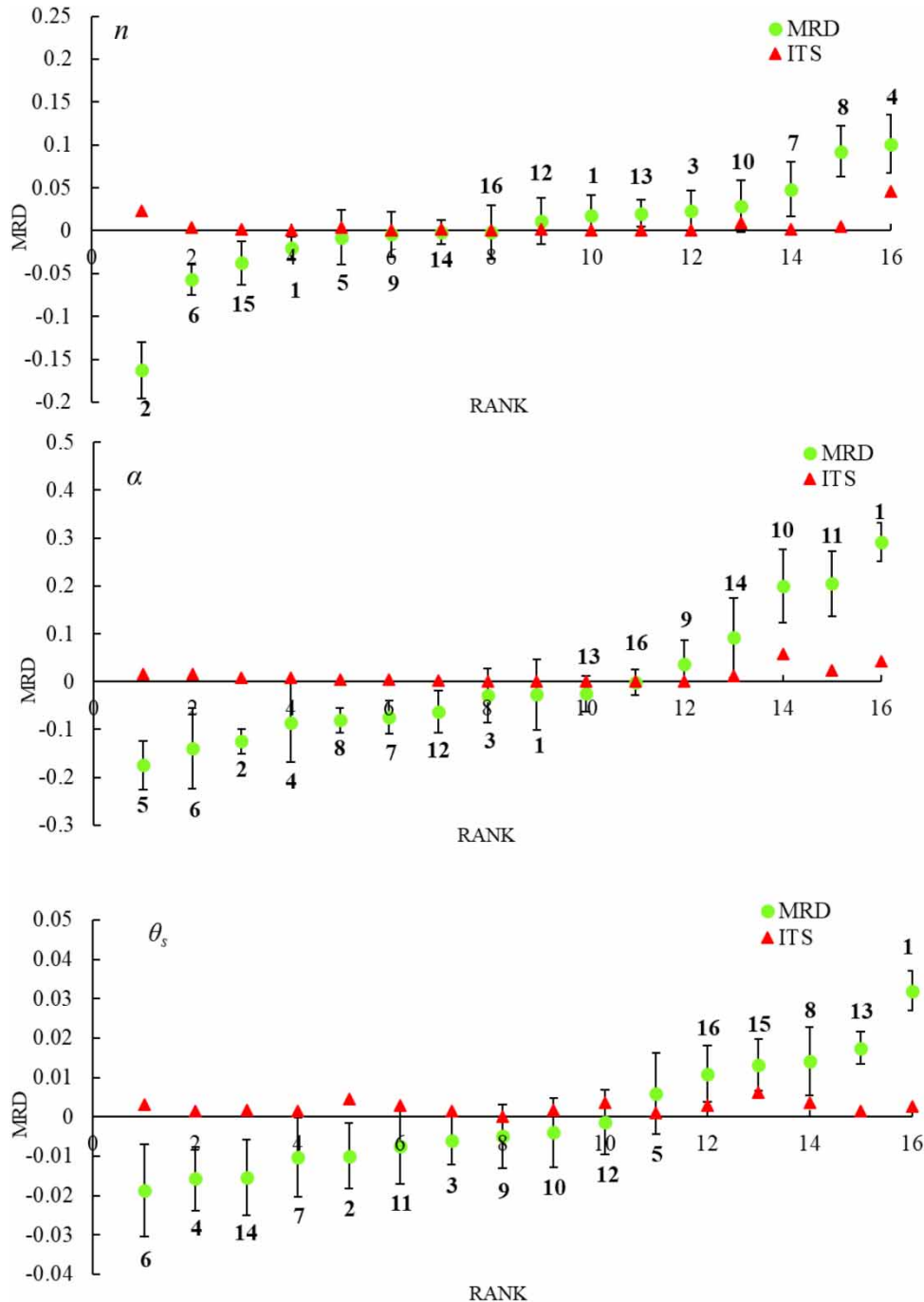


**Figure 4** | SDRD and ITS of soil moisture at 0–10 cm measuring point (note: the number on the error line is the sampling point number, the error line is the standard deviation of MRD (SDRD) of parameters, the red points represent the index of temporal stability (ITS) of parameters, the green points represent the MRD of parameters, rank in linear algebra (Rank)). The full colour versions of the figures are available in the online version of this paper, at http://dx.doi.org/10.2166/ws.2021.316

### Correlations between the soil layers and the SWCC parameters

The authors determined the correlations between the SWCC parameters and the 0–10, 10–20, and 20–30 layers (Table 2). $\alpha$, $n$ and $\theta_s$ were all strongly significantly correlated positively, with correlation coefficients of adjacent layers >0.749. Determining SWCC for the surface layer of the representative point helped the study of soil-water movement and solute transport (Mohammadi & Vanclooster 2010; Golian *et al.* 2020). SWCC plays an important role in estimating shear strength and the coefficients of unsaturated permeability, diffusion and adsorption.

### Analysis of temporal stability

#### Comparison of MRD, SDRD and ITS

The model parameters $\alpha$, $n$, and $\theta_s$ at the 16 sampling points in 2019 are sorted by the mean relative difference (MRD) in order to represent the temporal stability of the SWCC parameters at a depth of 0–10 cm. The green points represent the mean relative difference (MRD). The black error line is the standard deviation of MRD (SDRD). The red points represent the index of temporal stability (ITS) of parameters (Figure 4). SDRD for $\alpha$, $n$ and $\theta_s$ was 0.0263–0.0845, 0.0126–0.0337 and 0.0040–0.0117, respectively. SDRD for $\theta_s$ for most measurement points was <10%, similar to the results reported by Liu *et al.* (2014). MRD for $\alpha$, $n$ and $\theta_s$ was −0.1749–0.2913, −0.1625–0.1013、 and −0.0188–0.0319, respectively.

Determining one or a few sampling points where SWCC is the most temporally stable can decrease cost or increase sampling frequency and can be used to estimate the overall field SWCC. Several studies have successfully identified representative points and have estimated the conditions of SWC for study areas (Zucco *et al.* 2014; Zhao *et al.* 2017). The representative point with a mean relative difference closest to zero and with the lowest SD can be used to estimate the mean SWC of an experimental area (Bai & Shao 2011). The authors thus selected the point with the lowest ITS, which considers both the MRD and the SDRD, as the most representative point in our study (Figure 4). $\alpha$, $n$ and $\theta_s$ the observation points of the MRDs to 0 were 16, 16 and 12 respectively. However, the SDRDs for these points were not the lowest. $\alpha$, $n$ and $\theta_s$ the observation points of the lowest SDRDs were 2, 11 and 13 respectively. The authors had no observation points for the SWCC parameters, and both of the above conditions were met. So the authors introduced the ITS to assist in identifying the representative measurement points, thereby obtaining the lowest ITS values. The observation points were 16, 16 and 9.

#### Representative sampling point

The goodness of fit of the representative sample points identified by the above three methods was analyzed to obtain a statistical table for the VG fitting curve of the representative measuring points of the layers (Table 3). A comparison of the

**Table 3** | Statistical table of V-G fitting curve of representative measuring points of soil layer

| No. of measuring point | Soil layer (cm) | V G model | $R^2$ | Residual square | SD |
|---|---|---|---|---|---|
| 2 | 0–10 | $\theta(s) = 0.1191 + 0.3200/(1 + 0.0024s^{2.4005})^{0.5834}$ | 0.9465 | 0.1001 | 0.0265 |
|  | 10–20 | $\theta(s) = 0.1345 + 0.3050/(1 + 0.0024s^{2.5992})^{0.6153}$ | 0.9500 | 0.0899 | 0.0251 |
|  | 20–30 | $\theta(s) = 0.1357 + 0.3164/(1 + 0.0027s^{2.3924})^{0.5820}$ | 0.9474 | 0.0923 | 0.0254 |
| 9 | 0–10 | $\theta(s) = 0.1484 + 0.2796/(1 + 0.0028s^{2.8835})^{0.6532}$ | 0.9702 | 0.0558 | 0.0198 |
|  | 10–20 | $\theta(s) = 0.1527 + 0.2717/(1 + 0.0028s^{2.7807})^{0.6404}$ | 0.9637 | 0.0652 | 0.0214 |
|  | 20–30 | $\theta(s) = 0.1501 + 0.2759/(1 + 0.0024s^{2.9387})^{0.6597}$ | 0.9614 | 0.0677 | 0.0218 |
| 11 | 0–10 | $\theta(s) = 0.1593 + 0.2788/(1 + 0.0035s^{2.8642})^{0.6509}$ | 0.9495 | 0.0946 | 0.0257 |
|  | 10–20 | $\theta(s) = 0.1686 + 0.2519/(1 + 0.0034s^{2.9508})^{0.6611}$ | 0.9325 | 0.1214 | 0.0291 |
|  | 20–30 | $\theta(s) = 0.1629 + 0.2686/(1 + 0.0033s^{2.6917})^{0.6285}$ | 0.9529 | 0.0827 | 0.0240 |
| 12 | 0–10 | $\theta(s) = 0.1428 + 0.2842/(1 + 0.0027s^{2.7826})^{0.6406}$ | 0.9715 | 0.0533 | 0.0193 |
|  | 10–20 | $\theta(s) = 0.1497 + 0.2809/(1 + 0.0026s^{2.8675})^{0.6513}$ | 0.9661 | 0.0610 | 0.0206 |
|  | 20–30 | $\theta(s) = 0.1560 + 0.2709/(1 + 0.0026s^{2.9643})^{0.6626}$ | 0.9630 | 0.0650 | 0.0211 |
| 13 | 0–10 | $\theta(s) = 0.1454 + 0.2935/(1 + 0.0027s^{2.9396})^{0.6598}$ | 0.9710 | 0.0542 | 0.01947 |
|  | 10–20 | $\theta(s) = 0.1501 + 0.2823/(1 + 0.0026s^{2.9630})^{0.6625}$ | 0.9660 | 0.0612 | 0.0207 |
|  | 20–30 | $\theta(s) = 0.1550 + 0.2806/(1 + 0.0026s^{3.1293})^{0.6804}$ | 0.9631 | 0.0653 | 0.0211 |
| 16 | 0–10 | $\theta(s) = 0.1454 + 0.2813/(1 + 0.0027s^{2.9129})^{0.6567}$ | 0.9718 | 0.0529 | 0.0192 |
|  | 10–20 | $\theta(s) = 0.1513 + 0.2775/(1 + 0.0027s^{2.8504})^{0.6492}$ | 0.9662 | 0.0608 | 0.0206 |
|  | 20–30 | $\theta(s) = 0.1532 + 0.2890/(1 + 0.0028s^{2.7723})^{0.6393}$ | 0.9634 | 0.0643 | 0.0212 |
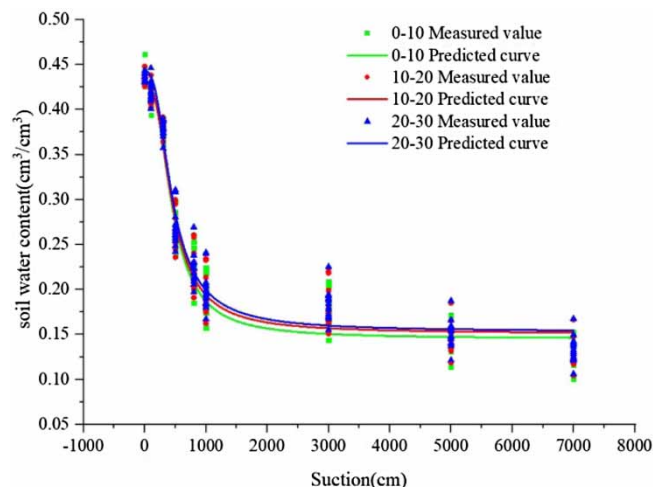
**Figure 5** | SWCC of representative measuring points.

coefficients of determination ($R^2$) and residual square for each layer indicated that $R^2$ was highest for measurement point 16, at 0.9718, 0.9662 and 0.9634, for the 0–10, 10–20 and 20–30 cm layers, respectively. The residual squared were lowest at 0.0529, 0.0608 and 0.0643 for the 0–10, 10–20 and 20–30 cm layers, respectively. SWCC and the measured values at measuring point 16 in the layers are shown in Figure 5. The measured points were evenly distributed on both sides of the curve. A single sampling point could thus be used to accurately estimate the field mean SWCC. The identification of representative measurement points of SWCC for collapsible loess because it can reduce the sample size while maintaining a high accuracy of prediction. So the prevention of loss of soil and water on the Loess Plateau provides a fast and efficient monitoring method.

## CONCLUSION

In this study, the spatiotemporal variability and the representative measurement points of SWCC parameters in the collapsible loess region were analyzed using the mean relative differences (MRD), standard deviation (SDRD), and index of temporal stability (ITS). The SWCC parameter $\alpha$ was moderately variable, $n$ and $\theta_s$ were weakly variable in the layers. The $CVs$ gradually increased with depth. The analysis of the standard deviations indicated that $\alpha$, $n$ and $\theta_s$ did not differ significantly between the layers. $\alpha$, $n$ and $\theta_s$ were strongly significantly correlated positively in the layers, with correlation coefficients between adjacent layers >0.749. Point 16 was identified as the point most representative of the SWCC, with the lowest cumulated ITS. The representative point was quite reliable for estimating the SWCC, with the highest $R^2$ of 0.9718 and the residual squared of 0.0529.

This study has contributed to our understanding of SWCC spatiotemporal patterns in the collapsible loess area in northwestern China. The results can be effectively used to design sampling schemes for SWCC measurements and provide theoretical guidance for soil water management and other applications.

## ACKNOWLEDGEMENTS

## DATA AVAILABILITY STATEMENT

All relevant data are included in the paper or its Supplementary Information.

## REFERENCES

Bai, Y. R. & Shao, M. A. 2011 Temporal stability of soil water storage on slope in rainfed region of Loess Plateau. *Transactions of the Chinese Society of Agricultural Engineering* **27** (7), 45–50. doi: 10.3969/j.issn.1002-6819.2011.07.008.

Brocca, L., Tullo, T., Melone, F. & Morbidelli, R. 2012 Catchment scale soil moisture spatial-temporal variability. *Journal of Hydrology* **422–423**, 63–75. doi: 10.1016/j.jhydrol.2011.12.039.

Chen, H. B. 2004 Hillslope-scale spatial variability of some soil properties. *Bulletin of Soil and Water Conservation* **24** (6), 45–48. doi: 10.3969/j.issn.1000-288X.2004.06.012.

Coppola, A., Comegna, A., Dragonetti, G., Lamaddalena, N., Kader, A. M. & Comegna, V. 2011 Average moisture saturation effects on temporal stability of soil water spatial distribution at field scale. *Soil & Tillage Research* **114** (2), 155–164. doi: 10.1016/j.still.2011.04.009.

Derakhshannia, M., Dalvand, S., Asakereh, B. & Askari, K. 2020 Corrosion and deposition in Karoon River, Iran, based on hydrometric stations. *International Journal of Hydrology Science and Technology* **10** (4), 334–345. http://dx.doi.org/10.1504/IJHST.2020.108264.

Genuchten V, T. M. 1980 A closed-form equation for predicting the hydraulic conductivity of unsaturated soils. *Soilence Society of America Journal* **44** (5), 892–898. doi: 10.2136/sssaj1980.03615995004400050002x.

Golian, M., Katibeh, H., Singh, V., Ostad-Ali-Askari, K. & Rostami, H. 2020 Prediction of tunnelling impact on flow rates of adjacent extraction water wells. *Quarterly Journal of Engineering Geology and Hydrogeology. The Geological Society of London, UK* **53** (2), 236. https://doi.org/10.1144/qjegh2019-055.

Haeri, S. M., Garakani, A. A., Roohparvar, H. R., Chandrakant, S. D., Ghafouri, S., Dist M ASCEGhafouri, M. H. S. & Kouchesfahani, K. S. 2019 Testing and constitutive modeling of lime-stabilized collapsible loess. I: experimental investigations. *International Journal of Geomechanics* **19** (4), 04019006–040190010. doi: 10.1061/(ASCE)GM.1943-5622.0001364.

Idrysy, E. H. E. & Smedt, F. D. 2007 A comparative study of hydraulic conductivity estimations using geostatistics. *Hydrogeology Journal* **15** (3), 459–470. doi: 10.1007/s10040-007-0166-0.

Jacobs, J. M., Hsu, E. C. & Choi, M. 2010 Time stability and variability of electronically scanned thinned array radiometer soil moisture during Southern Great Plains hydrology experiments. *Hydrological Processes* **24** (19), 2807–2819. doi:10.1002/hyp.7703.

Li, H. C., Tao, J. L., Wei, L. Y. & Yan, Z. L. 2019 Explosive compaction technology for loess embankment settlement control: numerical simulation and field implementation. *Acta Geotechnica* **15**, 975–997. doi: 10.1007/s11440-019-00777-y.

Lin, Q. & Xu, S. H. 2018 Parameter identification and uncertainty analysis of soil water movement model in field layered soils based on Bayes Theory. *Journal of Hydraulic Engineering* **49** (4), 428–438. doi: 10.13243/j.cnki.slxb.2017099.

Liu, J. L., Ma, X. Y., Zhang, Z. H. & Fu, Q. 2014 Temporal stability of soil moisture in an orchard. *Journal of Basic Science and Engineering* **22** (4), 698–704. doi: 10.3969/j.issn.1005-0930.2014.04.007.

Liu, X. Z., Li, J. Z. & Zhang, Z. H. 2007 A new method to estimating parameters of Van Genuchten model for soil water retention. *Acta Pedologica Sinica* **44** (6), 1135–1138. doi: 10.3321/j.issn:0564-3929.2007.06.025.

Lv, M., Li, Y. & Guo, Y. 2021 Water retention characteristics and soil-water characteristic curve model of weak expansive soil. *Soil Mechanics and Foundation Engineering* **58** (2), 123–129. doi: 10.1007/s11204-021-09716-0.

Mohammadi, M. H. & Vanclooster, M. 2010 Analysis of flow rate dependency of solute transport in an undisturbed inceptisol. *Vadose Zone Journal* **10** (1), 394–402. doi: 10.2136/vzj2010.0046.

Ng, C. W. W., Mu, Q. Y. & Zhou, C. 2017 Effects of soil structure on the shear behaviour of an unsaturated loess at different suctions and temperatures. *Canadian Geotechnical Journal* **54** (2), 270–279. doi: 10.1139/cgj-2016-0272.

Oliver, M. A. & Webster, R. 2014 A tutorial guide to geostatistics: computing and modelling variograms and kriging. *Catena* **113** (2), 56–69. doi: 10.1016/j.catena.2013.09.006.

Olyphant, G. A. 2003 Temporal and spatial (down profile) variability of unsaturated soil hydraulic properties determined from a combination of repeated field experiments and inverse modeling. *Journal of Hydrology* **281** (1), 23–35. doi: 10.1016/S0022-1694(03)00198-7.

Ostad-Ali-Askari, K., Su, R. & Liu, L. 2018a Water resources and climate change. *Journal of Water and Climate Change* **9** (2), 239. https://doi.org/10.2166/wcc.2018.999.

Ostad-Ali-Askari, K., Shayannejad, M., Eslamian, S. & Navabpour, B. 2018b Comparison of solutions of Saint-Venant equations by characteristics and finite difference methods for unsteady flow analysis in open channel. *International Journal of Hydrology Science and Technology* **8** (3), 229–243. doi: 10.1504/IJHST.2018.093569.

Penna, D., Brocca, L., Borga, M. & Dalla Fontana, G. 2013 Soil moisture temporal stability at different depths on two alpine hillslopes during wet and dry periods. *Journal of Hydrology* **477** (1), 55–71. doi: 10.1016/j.jhydrol.2012.10.052.

Pham, T. D. 2016 The Semi-Variogram and spectral distortion measures for image texture retrieval. *IEEE Trans Image Process* **25** (4), 1556–1565. doi: 10.1109/TIP.2016.2526902.

Shen, J., Hu, M. J., Wang, X., Zhang, C. Y. & Xu, D. S. 2021 SWCC of calcareous silty sand under different fines contents and dry densities. *Frontiers in Environmental Science* **9**, 303. doi:10.3389/fenvs.2021.682907.

Vachaud, G. A., Silans, A. P. D., Balabanis, P. & Vauclin, M. 1985 Temporal stability of spatially measured soil water probability density function1. *Soil Science Society of America Journal* **49** (4), 822–828. doi: 10.2136/sssaj1985.03615995004900040006x.

Vanani, H. R., Shayannejad, M., Tudeshki, A. R. S., Ostad-Ali-Askari, K., Eslamian, S., Mohri-Esfahani, S., Mohri-Esfahani, E., Haeri-Hamedani, M. & Jabbari, H. 2017 Development of a new method for determination of infiltration coefficients in furrow irrigation with natural non-uniformity of slope. *Sustainable Water Resources Management* **3** (2), 163–169. https://doi.org/10.1007/s40899-017-0091-x.

Wang, S. J., Cheng, M. S., Li, X., Wang, X. Q., Mao, X. & Yang, H. D. 2017 Establishment of generalized soil-water characteristic curve theoretical model considering two stress state variables for unsaturated soils. *Transactions of the Chinese Society of Agricultural Engineering (Transactions of the CSAE)* **33** (6), 1–7. doi: 10.11975/j.issn.1002-6819.2017.06.001.

Wen, J., Han, J. L., Yao, L. H. & Li, L. J. 2015 Study of hydraulic conductivity of unsaturated loess in-situ conditions. *Rock and Soil Mechanics* **36** (9), 172–179. doi: 10.16285/j.rsm.2015.09.021.

Wraith, J. M. 2004 Soil water dynamics. *Vadose Zone Journal* **3** (4), 1490–1490. doi: 10.2136/vzj2004.1490.

Xing, Y. C., Li, J. S. & Li, Z. 2007 Deformation characteristics of collapsible loess and expansive soil under the condition of wetted in stages. *Journal of Hydraulic Engineering* **38** (5), 546–551. doi: 10.1016/S1872-583X(07)60011-4.

Yan, Y. J. & Wen, B. P. 2013 Structural yielding characteristics of unsaturated loess and main influencing factors. *Hydrogeology and Engineering Geology* **40** (3), 63–68. doi: 10.16030/j.cnki.issn.1000-3665.2013.03.009.

Yun-Xue, Y. E., Zou, W. L., Han, Z. & Liu, X. W. 2019 Predicting the entire soil-water characteristic curve using measurements within low suction range. *Journal of Mountain Science* **16** (05), 1198–1214. doi: CNKI:SUN:SDKB.0.2019-05-018.

Zhang, Z. B. & Peng, X. H. 2015 A review of researches on sail cracks and their impacts on preferential flow. *Acta Pedologica Sinica* **52** (3), 477–488. doi:10.11766/trxb201409030446.

Zhang, A. J., Wang, Y. G., Xing, Y. C., Yu, C. L. & Zhao, Q. Y. 2019 Fitting models for soil-water characteristic curve of total and matrix suctions of Yili loess. *Chinese Journal of Geotechnical Engineering* **41** (6), 1040–1049. doi:10.11779/CJGE201906007.

Zhao, W. J., Cui, Z., Zhang, J. Y. & Jin, J. 2017 Temporal stability and variability of soil-water content in a gravel-mulched field in northwestern China. *Journal of Hydrology* **552**, 249–257. doi: 10.1016/j.jhydrol.2017.06.031.

Zhao, W. J., Cao, T. H., Li, Z. L., Su, Y. & Bao, Z. W. 2020 Spatial variability of the parameters of soil-water characteristic curves in gravel-mulched fields. *Water Science and Technology-Water Supply* **20** (1), 231–239. doi: 10.2166/ws.2019.153.

Zucco, G., Brocca, L., Moramarco, T. & Morbidelli, R. 2014 Influence of land use on soil moisture spatial-temporal variability and monitoring. *Journal of Hydrology* **516** (6), 193–199. doi: 10.1016/j.jhydrol.2014.01.043.